



Communication

Eco-friendly and recyclable all cellulose triboelectric nanogenerator and self-powered interactive interface[☆]Jintao Zhang^{a,b,1}, Sanming Hu^{c,1}, Zhijun Shi^{c,1}, Yifei Wang^{b,d}, Yanqiang Lei^b, Jing Han^b, Yao Xiong^b, Jia Sun^e, Li Zheng^a, Qijun Sun^{b,d,f,*}, Guang Yang^{c,**}, Zhong Lin Wang^{b,d,g,*}^a School of Mathematics and Physics, Shanghai Key Laboratory of Materials Protection and Advanced Materials in Electric Power, Shanghai University of Electric Power, Shanghai 200090, PR China^b Beijing Institute of Nanoenergy and Nanosystems, Chinese Academy of Sciences, Beijing 101400, PR China^c College of Life Science and Technology, Huazhong University of Science and Technology, Wuhan 430074, PR China^d School of Nanoscience and Technology, University of Chinese Academy of Sciences, Beijing 100049, PR China^e School of Physics and Electronics, Central South University, Changsha 410083, PR China^f Center on Nanoenergy Research, School of Physical Science and Technology, Guangxi University, Nanning 530004, PR China^g School of Materials Science and Engineering, Georgia Institute of Technology, Atlanta, GA 30332-0245, United States

ARTICLE INFO

Keywords:

All-cellulose TENG
Bacterial cellulose
Energy harvesting
Eco-friendly
Self-powered interface

ABSTRACT

Environment issues calls for eco-friendly, recyclable, and biodegradable natural materials for the extensive application of distributed energy harvesting triboelectric nanogenerators (TENGs) and wearable self-powered interfaces. Biocompatible bacterial cellulose (BC) with high crystallinity, good mechanical properties and distinctive porous network is ready to construct biodegradable and eco-friendly TENGs. Here, we develop an eco-friendly and recyclable all-cellulose energy-harvesting and interactive device based on sandwich-structured BC-TENG. It is composed of pure BC and conductive BC precipitated with conducting and reinforced nanomaterials as friction layers and electrodes, respectively. Degradation experiments are conducted in this work to demonstrate the active materials can be completely degraded within 8 h under the condition of cellulolytic enzyme. We have also carefully investigated the output performances of the prepared all-cellulose TENG, which shows a maximum open-circuit voltage of 29 V, short-circuit current of 0.6 μ A, and output power at 3 μ W. The all-cellulose TENG is readily utilized to power commercial electronics and functionalize as a wearable sewing interface to control an electronic piano. This work provides an efficient route to preparing all-cellulose energy-harvesting and interactive device with good biodegradability, which is of great importance in eco-friendly electronics, bio-adaptive human-machine interfaces and intelligent biomimetic functional devices.

1. Introduction

Triboelectric nanogenerator (TENG), driven by Maxwell's displacement current, delivers a killer means toward harvesting low-frequency and high-entropy mechanical energy from surrounding environment [1–8]. It is also readily utilized for active interactive interface based on the TENG device itself [9–13], tribotronic transistor [14–17], triboiontronics [18–20] and mechanoplastic sensory neurons [21–28]. Thanks to the facile design, simple structure, and diverse materials choice, it is

qualified to be a fundamental energy source demanded for the new era of IoTs, involving distributed micro-power suppliers for sensory nodes, wearable self-powered systems, portable high-voltage power, and even potential state-grid of blue energy [29–33]. Generally, non-noble metals and plastic polymers are commonly chosen as the electrodes and friction materials to fabricate the TENGs [34]. However, these metals (e.g., copper and aluminium) [35,36] are susceptible to be corroded into $\text{Cu}^+/\text{Cu}^{2+}$ and Al^{3+} to contaminate water and soil, and most plastic polymers cannot be completely degraded and have risk to release

[☆] Prof Zhong Lin Wang, an author on this paper, is the Editor-in-Chief of Nano Energy, but he had no involvement in the peer review process used to assess this work submitted to Nano Energy. This paper was assessed, and the corresponding peer review managed by Professor Chenguo Hu, an Associate Editor in Nano Energy.

* Corresponding authors at: Beijing Institute of Nanoenergy and Nanosystems, Chinese Academy of Sciences, Beijing 101400, PR China.

** Corresponding author.

E-mail addresses: sunqijun@binn.cas.cn (Q. Sun), yang_sunny@yahoo.com (G. Yang), zhong.wang@mse.gatech.edu (Z.L. Wang).

¹ These authors contributed equally: Jintao Zhang, Sanming Hu, Zhijun Shi.

hazardous chemicals after decomposition. Regarding to the environment issues and electronic wastes, it is highly desired to develop eco-friendly, recyclable, and biodegradable natural materials for the extensive application of distributed energy harvesting TENGs and wearable self-powered interfaces [37–43]. Relevant studies concerning on the development of green materials with related devices have been intensively conducted toward the worldwide emerging trend of carbon neutrality.

A biodegradable TENG has been made of synthetic polymers to work as a life-time designed implantable power source [44]. The replacement rate of related power sources inevitably causes heavy financial burden, poor experience for users, and critical physical pains to patients [45–48]. Further considering the degradable synthetic polymers are nonrenewable with complex composition, researchers have been seeking for proper natural materials (e.g., alginate, rice paper, cotton, etc.) to prepare the biodegradable and eco-friendly TENG [49–51]. Cellulose, the most abundant natural polymer on earth, has been chosen as friction materials to achieve eco-friendly TENG with good biodegradability, biocompatibility and flexibility [52–54]. Specially, bacterial cellulose (BC) is one type of natural celluloses produced by bacteria, which possesses distinctive three dimensional porous network and crystalline nanofibrils with diameters at 10–100 nm [55–57]. Compared with the vegetal cellulose, BC shows the advantages of higher purity/crystallinity/porosity, permeability to liquid and gases, better biocompatibility, and more excellent mechanical robustness [58–61]. Moreover, it is facile to make chemical/physical surface modification on BC due to the existence of widely distributed -OH groups and porous network structures [55]. By modifying BC with conducting polymers (e.g., polypyrrole (PPy), and polyaniline (PANI)), carbon nanotubes (CNTs), graphene or other functional molecules/coatings, it can be readily reinforced to work as versatile hydrogels, biosensors, supercapacitors, and bioelectronics interface [61–64]. Thus, with only BC derived materials, it is applicable to construct a material/structure-facile, low-cost and eco-friendly TENG, adopting pure BC and conductive BC as friction materials and electrodes, respectively. Sophisticated selection/preparation of BC materials supplies a promisingly new way for developing eco-friendly TENGs and potential self-powered bio-interfaces.

Here, we develop an eco-friendly and recyclable all-cellulose energy-harvesting and interactive device based on a BC-CNT-PPy/BC/BC-CNT-PPy sandwich-structured TENG, which is composed of pure BC and conductive BC precipitated with CNT/PPy as friction layers and electrodes, respectively. High-purity BC membrane produced by inoculated *Gluconacetobacter hansenii* is used as one of the friction layers, while CNT/PPy incorporated and reinforced conductive BC membrane is used as the other friction layer. Both of the BC materials are characterized and analyzed in details. The biodegradation experiments are conducted to demonstrate that BC and BC-CNT-PPy membranes can be degraded within 8 h under the condition of cellulolytic enzyme and the left CNTs is available to be collected for reuse. We also systematically investigate the output performance of fabricated all-cellulose TENG in different parameters (e.g., resistance of the conductive BC membrane, size of the BC friction layer, and contact-separation frequency). The all-cellulose TENG shows a maximum open-circuit voltage of 29 V, short-circuit current of 0.6 μ A, and output power at 3 μ W with paired resistance at 25 M Ω . Finally, the all-cellulose TENG is successfully used to power commercial electronic devices and functionalize as a wearable sewing interactive interface to control an electronic piano. This work provides an efficient route to preparing all-cellulose energy-harvesting and interactive device with good eco-friendly properties. The biomaterials derived TENG is believed to have great significance in eco-friendly electronics, bio-adaptive energy harvesting devices, wearable human-machine interface and even biomimetic functional artificial electronic organs.

2. Results and discussion

Fig. 1a illustrates the detailed preparation process of the pure BC membranes and CNT/PPy reinforced conductive BC membranes (BC-CNT-PPy). At first, *Gluconacetobacter Hansenii* [65] capable of producing cellulose in high purity, good crystallinity, and excellent mechanical stability is selected to be firstly inoculated and cultured in the culture medium (containing disodium hydrogen phosphate dodecahydrate, peptone, yeast extract, citric acid, and glucose). After rinsing in pure water for three days, the obtained BC membrane (thickness, \sim 0.1 mm) is treated by boiling in NaOH solution to remove any medium and adsorbed bacteria with subsequent oven drying process for further use. To prepare BC-CNT-PPy, CNT is firstly incorporated into the highly swollen BC pellicle by repeated immersion/sonication/shaking in a MWCNT dispersion and obtain the BC-CNT composite pellicle. The successful incorporation of CNTs can be testified by the color changes from a white to a dark color (Fig. S1). Ferric (III) ion is used as an oxidant for in-situ oxidative polymerization of pyrrole to PPy prepare the BC-CNT-PPy membrane. After removing the physically adsorbed water by mechanical pressing, the obtained BC-CNT composite pellicle is immersed in a ferric (III) ion solution under magnetic stirring for 2 h, then immersed in the pyrrole solution and stirred at 4 $^{\circ}$ C for 60 min to initiate the polymerization of polypyrrole and obtain BC-CNT-PPy composite pellicles. Finally, the BC-CNT-PPy composite membranes are prepared by hot-pressing the BC-CNT-PPy composite pellicles under 120 $^{\circ}$ C for 6 h (thickness, \sim 0.16 mm, more detailed fabrication process is in the Experiment part and Fig. S2). Thus, both pure BC and CNT/PPy reinforced conductive BC membranes are obtained to fabricate the all-cellulose based TENG. Fig. 1b shows the schematic illustration of the all-cellulose TENG in contact-separation mode, with BC membrane as one friction layer and BC-CNT-PPy membranes as electrode and the other friction layer, respectively. Fig. 1c reveals scanning electron microscopy (SEM) images of BC, BC-CNT, BC-CNT-PPy and corresponding enlarged portion, respectively. From the image Fig. 1c (I), we can see that the pure BCs possess exquisite three-dimensional network structure, which facilitates its physical or chemical modification to form functional composites. Therefore, the CNT with the cetyltrimethylammonium bromide (CTAB) surfactant can easily infiltrate into the BC pellicles. As is shown in Fig. 1c (II), the bright regions in the images are ascribed to the MWCNTs due to their high conductivity, and the MWCNTs are densely absorbed onto the surface of the BC pellicles and distributed homogeneously without aggregation. After in-situ polymerization of polypyrrole, the diameters of bacterial cellulose nanofibers vary from \sim 50 nm in pure BC membranes to 100 nm in BC-CNT-PPy membranes (Fig. 1c (III)). This obvious change is due to that PPy deposited on the surface of BC forms a core-shell structure. Fig. 1c (IV), (V) and (VI) corresponds to the details of Fig. 1c (I), (II), and (III), respectively. The interaction between hydrogen bonds of BC and -NH of pyrrole ring helps to prevent self-aggregation of PPy nanoparticles [52]. The homogeneous dispersion of CNTs and deposition of PPy nanoparticles in BC matrix is one of the most important requirements for achieving a uniform conductivity. Corresponding mechanical and conductive properties of BC-CNT-PPy membrane are discussed in Fig. S3. Fig. S3a and b are the stress-strain curve and tensile modulus of pure BC, BC-CNT, and BC-CNT-PPy composite membrane. We can know that the incorporation of CNT increases the mechanical strength of BC membrane, while the in-situ polymerization of polypyrrole reduces mechanical strength of BC-CNT composite. This is because the incorporation of CNT effectively fills the network structure of BC, while polypyrrole forms a shell-sheath structure on the BC nanofiber, making the BC membrane sparser. Fig. S3c is thermogravimetric analysis (TGA) of pure BC, BC-CNT, and BC-CNT-PPy composite membrane. With the incorporation of CNT and polypyrrole polymerization, the thermal stability of the materials is gradually increased, because CNTs can effectively absorb heat, and polypyrrole forms a shell and sheath structure on the BC fiber so that the BC fiber is expected to be less exposed to thermal shock. BC-CNT-PPy

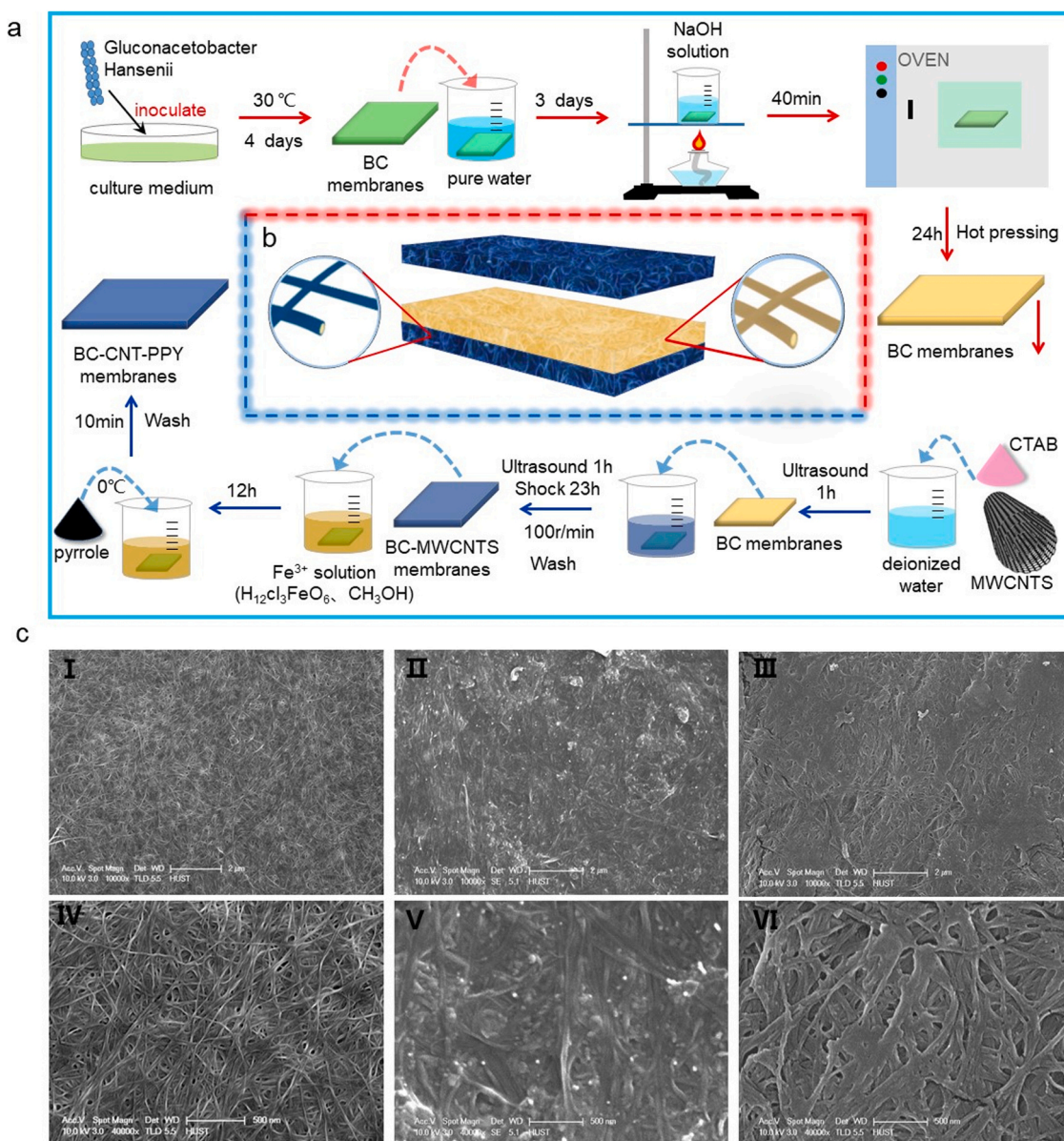


Fig. 1. (a) Schematic illustration of pure BC membrane and conductive BC-CNT-PPy composite membrane fabrication. (b) Schematic image of the TENG's structure. (c) SEM images of prepared membranes, I) pure BC membrane, II) BC-CNT membrane, III) BC-CNT-PPy membrane, and IV)-VI) enlarged images of I)-III).

membrane shows good electrical conductivity compared with BC and BC-CNT samples (Fig. S3d).

Material properties related with chemical modification are critical to the output performance of TENG devices. To verify the changes in the surface chemical bonding, the prepared different BC membranes are firstly characterized by Fourier-transform infrared (FT-IR) spectroscopy. The FT-IR spectra of pure BC, BC-CNT and BC-CNT-PPy are shown in Fig. 2a. Pure BC has three absorption peaks: two peaks located at $\sim 3345\text{ cm}^{-1}$ and $\sim 2887\text{ cm}^{-1}$ are attributed to the stretching vibration of O-H and C-H. The peaks at 1642 cm^{-1} and 1045 cm^{-1} are attributed to the deformation vibration of O-H and C-O, respectively. After the incorporation of CNTs, the decreased intensity for all the characteristic peaks is observed. A newly introduced peak at 798 cm^{-1} corresponds to an enhanced C-H stretching vibration, further confirming the fact of CNTs incorporation. With pyrrole further polymerized on BC-CNT membrane, the characteristic adsorption peak of C=C stretching vibration of pyrrole ring is observed at 1550 cm^{-1} [58,66]. Besides, the curve of BC-CNT-PPy shows the characteristic peaks belong to polypyrrole at around 1550 cm^{-1} and 1455 cm^{-1} , corresponding to C-N

stretching vibration and C-C stretching vibrations in the pyrrole ring, respectively [66]. Compared with the absorption bands of BC-CNT and BC-CNT-PPy (Fig. 2b), we find that the peak intensity is also significantly reduced in the wavenumber ranged from ~ 1300 to $\sim 700\text{ cm}^{-1}$, indicating that there is a strong interaction between CNT-PPy and BC. To further corroborate the chemical modification process of CNT/PPy incorporation, X-ray photoelectron spectroscopy (XPS) for pure BC, BC-CNT and BC-CNT-PPy membranes are conducted. The contrast wide scans showed in Fig. 2c display that all membranes have binding energies (BE) consistent with carbon 1s (C 1s) and oxygen 1s (O 1s) core-shells, exhibiting an obvious increment in carbon after CNT loading along with an expected escalating difference in C 1s/O 1s, as duly marked in the spectrum. The existence of a nitrogen 1s core-shell (N 1s) in BC-CNT-PPy membrane reflects the efficient polymerization of the PPy on BC-CNT composites due to that only PPy is nitrogen-containing composition [66]. High-resolution scans of the N 1s is shown in Fig. 2d. In BC-CNT-PPy composite membranes, the N 1s core-level peak can be curve-fit into two peak components at 400.1 and 401.1 eV (ascribed to positively charged nitrogen $-\text{NH}^{2+}$ - and $-\text{NH}^{+}$ -), from which it can be

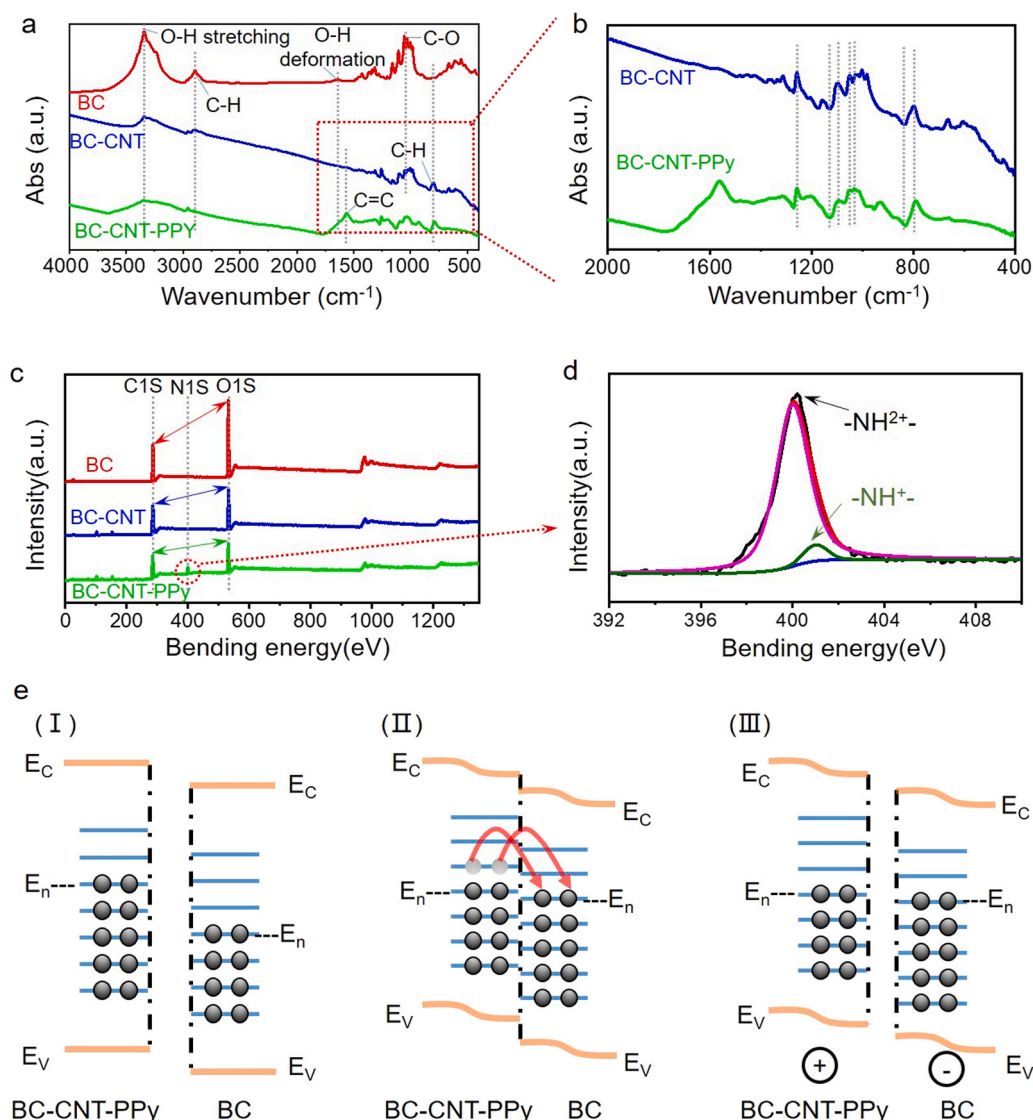


Fig. 2. (a) and (b) FTIR spectra of pure BC, BC-CNT, BC-CNT-PPy membranes. (c) and (d) XPS spectra of pure BC, BC-CNT, BC-CNT-PPy membranes. (e) Schematic illustration of the contact electrification mechanism between the pure BC and BC-CNT-PPy membrane.

inferred that the polymerization level of PPy measured on the surface is approximately 68%.

As is known, contact electrification (CE) in TENG is mainly dominated by electron transfer [67,68]. As the barrier height at the interface between two friction materials is a crucial factor for CE, the surface state models for the barrier height regulations are adopted to explain the CE mechanism between pristine BC and conductive BC. It is important to note that the barrier heights of materials correlate with their contacting materials and chemical compositions. The incorporation of CNTs and PPy in BC facilitates the ionic diffusion to significantly decrease the resistance. Meanwhile, CNTs with remarkable charge storage capacity, large aspect ratio and surface area act as conducting bridges between the pyrrole domains to enhance the electrical conductivity. CNTs can strongly interact with the aromatic rings in PPy chains to establish π -stacking and CH- π interactions and boost the overall electrical properties of the nanocomposite membrane. Therefore, the surface state (E_n) of BC-CNT-PPy is higher than that of pure BC (Fig. 2e (I)). Once there is a physical contact between the pure BC and BC-CNT-PPy, some electrons will cross a potential barrier and transfer from the conductive BC-CNT-PPy to the dielectric pure BC. Meanwhile, the potential barrier will be decreased by ΔE when the electrons transfer process is finished and enters an electric equilibrium state (Fig. 2e (II)). When the two

friction layers are separated, the BC-CNT-PPy is positively charged, while the pure BC is negatively charged (Fig. 2e (III)). The electric equilibrium state is changed and electrons will be driven by the potential difference to flow through external circuit. The illustrated surface state models can help to clarify the CE mechanism from the aspect of potential barrier heights modulation in the conductive and dielectric BCs and corresponding electron transfer process (Fig. S4).

Prior to the electrical characterization of the all-cellulose TENG outputs, corresponding simulations (finite element analysis) of the triboelectric potential distributions of the BC membranes in different resistances (100, 10, 2, and 0.3 k Ω) by COMSOL Multiphysics are shown in Fig. 3a to demonstrate the triboelectrification properties of different BC membranes. With more CNT and PPy incorporated in the BC membrane, it shows an enhanced conductivity and exhibits more electro-positive properties to lose electrons. In the simulated results, BC-CNT-PPy membrane with lower resistance shows more tendency to induce positive electrostatic field (or positive charges) upon contact-separation with pristine BC. Accordingly, the constructed TENG based on BC-CNT-PPy membrane in lower resistance (0.3 k Ω) shows an open circuit voltage (V_{OC}) of 19 V (contact-separation distance at \sim 5 cm, frequency at \sim 3 Hz). The V_{OC} gradually decreases to 4 V with the resistance of BC-CNT-PPy friction layer increased to 100 k Ω (Fig. 3b). Similarly, the short

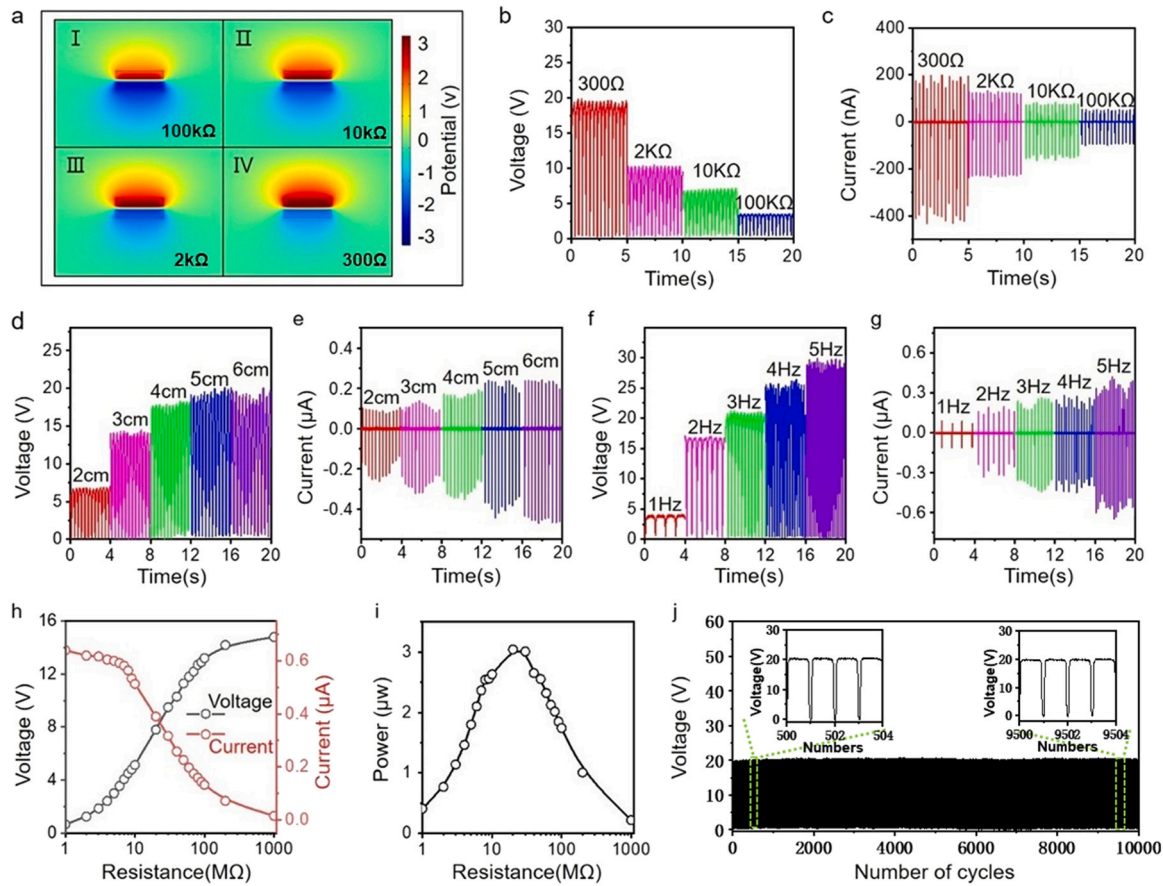


Fig. 3. (a) Schematic diagram of the simulation evolution of the electrostatic field when TENG works. (b) Voltage and (c) current output of the TENG with different resistance of the BC-CNT-PPy membrane. (d) Voltage and (e) current output of the TENG with different contact distance between friction layers. (f) Voltage and (g) current output of the TENG with different contact frequency. (h) Voltage and current output as a function of the load resistance. (i) Calculated output power as a function of the load resistance. (j) TENG output under periodic test for 10,000 cycles at 3 Hz.

circuit current (I_{SC}) decreases from 420 to 100 nA with the BC-CNT-PPy resistance decreased from 0.3 to 100 k Ω (Fig. 3c). Because the TENG with BC-CNT-PPy resistance at 0.3 k Ω shows the highest output, it is reasonably selected as the test sample in the following characterizations.

We characterize the output performances of the all-cellulose TENG upon different contact-separation distances and frequencies. As shown in Fig. 3d and 3e, both the V_{OC} and I_{SC} represent increment tendency with the contact-separation distance increased from 2 to 5 cm (contact frequency at 3 Hz). When the contact-separation distance is fixed at 6 cm, the output performance is similar with that of 5 cm. This may be attributed to that the TENG separation at 6 cm cannot efficiently lead to more significant electrostatic induction compared with the 5 cm separation case. For different contact-separation frequencies (increasing from 1 to 5 Hz with a separation distance at 5 cm), the V_{OC} and I_{SC} increase from 4 to 29 V and from 0.1 to 0.6 μ A, respectively. The achieved results above are consistent with the output evaluation equations of the TENG [10],

$$V_{OC} = \frac{\sigma x(t)}{\epsilon_0}$$

In this equation, ϵ_0 is permittivity of vacuum, x is the relative distance between the two friction layers. The output V_{OC} is determined by $x(t)$ and static charges density (σ), thereby proportional to the separation distance. When the separation distance dominates the output compared with the device size, the voltage V_{OC} may also deviate from the linear relationship.

Fig. 3f and g represent the V_{OC} and I_{SC} of the all-cellulose TENG at different contact frequencies (internal resistance is 300 Ω , contact-

separation distance is 5 cm), respectively. When the contact frequency is applied as 1 Hz, the V_{OC} and I_{SC} are 4 V and 0.1 μ A, respectively. When the frequency is increased to 2 Hz, both V_{OC} and I_{SC} have obvious increments. As the frequency continues to increase from 1 to 5 Hz, the V_{OC} also increases from 4 to 29 V and I_{SC} increases from 0.1 to 0.6 μ A. To evaluate I_{SC} , we can extract it from the equation as follows [69]:

$$I_{SC} = \frac{dQ_{SC}}{dt} = \frac{S\sigma d_0}{(d_0 + x(t))^2} \frac{dx}{dt} = \frac{S\sigma d_0 v(t)}{(d_0 + x(t))^2}$$

Here, Q is the transferred charge, S is the area size of the electrode, and σ is the density of the triboelectric charges. This equation means I_{SC} will be increased with the increment of static charge density σ and the contact-separation speed $v(t)$ between the two dielectrics. The output power of the all-cellulose TENG is also evaluated based on the output performances at different load resistances (contact distance is selected to be 5 cm and contact frequency is fixed at 3 Hz to get stable characteristics of the all-cellulose TENG). According to Ohm's law, as the load resistance increases, the potential drop (i.e., the output voltage) increases and the current flowing through the external circuit decreases (Fig. 3h). The output power (P) is calculated at different load resistances according to the equation of $P = U \times I$. The maximum output power is evaluated to be 3 μ W with the load resistance at 25 M Ω (Fig. 3i). As long-term stable output of TENG device is critical for practical and sustainable applications, the stability test of the all-cellulose TENG is shown in Fig. 3j. The output voltage can be maintained at a stable level for over 10,000 cycles of contact-separation. Insets of Fig. 3j further confirm the stable V_{OC} of \sim 20 V with almost no changes at the beginning and the end of the durability test. Considering it is the durability test, we

increase the contact frequency at 3 Hz and keep the separation distance at 5 cm. The input force is applied from 0.5 to 6 N in the whole experiment, and the details of the applied forces are shown in Fig. S5. The measured force increases with the increased contact frequency. This can be attributed to that the traction force in linear motor increases with the instrument settings according to the contact-separation frequency and is transmitted to the TENG device.

Due to the intrinsic hydrogel nature of BC with 3D crystalline network of macromolecular polysaccharide, BC and the precipitated conductive composites are ready to be biodegradable. And the left CNTs is available to be collected for reuse. The degradation experiments for pure BC membranes and BC-CNT-PPy composite membranes are conducted with enzymatic degradation method in cellulase solution, which is a type of basic and classical method to degrade bacterial cellulose [70]. The components of cellulase include cellobiohydrolase, endoglucanase, and β -glucanase. Cellobiohydrolase mainly acts on the surface of the nanofiber to crack the long cellulose molecular chain and free the end of the long chain molecule, thereby making the cellulose easy to hydrate; endoglucanase acts on cellulose activated by cellobiohydrolase to decompose its β -1, 4 glycosidic bonds to produce cellobiose, cello-triose and other short-chain oligosaccharides; the role of β -glucosidase is to decompose cellobiose and cello-triose into glucose [71]. Photo images of the real-time degradation process are in Fig. 4a and b. In the first two hours, the appearance of BC and BC-CNT-PPy films does not change significantly (Fig. S6). For the pure BC membrane (Fig. 4a), it starts to show a crimped shape combined with partial broken points after three hours. The color changes from white to translucent due to the decrease of crystallinity. At the fourth hour, the pure BC membrane is almost fully broken, at which stage the reinforced chains of BC are mostly depolymerized. In the subsequent four hours, the size of BC fragments

gradually decreases until almost complete disappearance at the eighth hour. Only some impurities and the corpse of *Acetobacter xylinum* are left, indicating the BC are fully depolymerized into soluble saccharide molecules. For the conductive BC-CNT-PPy membrane (Fig. 4b), the degradation takes place from all the edges and faster on the four corners, nearly maintaining the initial square shape but in a smaller size after three hours. This is because the network structure of the BC substrate is filled with CNT and PPy, which makes it difficult for cellulase molecules to penetrate into the interior and can only contact from the edge part of composite membrane. From the fourth hour, cracks start to show up at the edges and the BC-CNT-PPy membrane gets to be gradually degraded until all the BC composition is depolymerized in the subsequent four hours. Sugar concentration is an important index of degradation experiments [51]. To further indicate the degradation status, Fig. 4c and d present the curves of total sugar concentration and reducing sugar concentration during the degradation process for pure BC and BC-CNT-PPy composite membranes. The reducing sugar is glucose, and total sugars contain glucose and oligosaccharides (e.g., cellobiose and cello-triose). From the curve of reducing sugar concentration, the reducing sugar concentration values are almost the same in BC and BC-CNT-PPy during the measurement. From the curve of total sugar concentration, the concentration of total sugars in the degradation solution does not increase after the seventh hour, we can know that the pure BC and BC-CNT-PPy composite membranes are almost degraded within seven hours. The degradation rate of pure BC membranes is faster than the BC-CNT-PPy composite membranes in the first two hours from the curve of total sugar concentration in Fig. 4c. This is because that the BC-CNT-PPy composite membranes have tighter structure after incorporating CNT and coating PPy, which leads the cellulase more difficult to penetrate into the membrane at the beginning of degradation process.

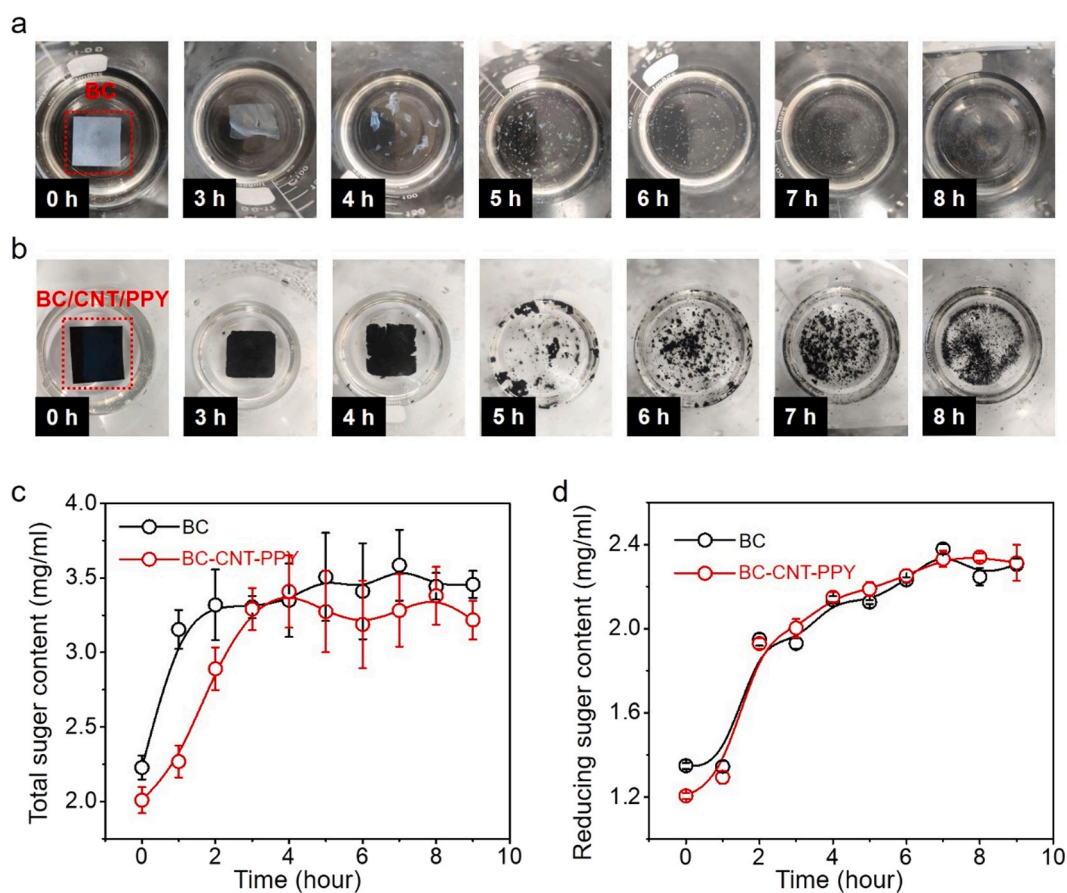


Fig. 4. (a) The digital photo of the degradation process of (a) pure BC and (b) BC-CNT-PPy membrane under cellulase. (c) Total sugar content and (d) reducing sugar content in the cellulase solution during degradation.

However, at the fourth hour of degradation process, the total sugar concentration and reducing sugar concentration for both BC and BC-CNT-PPy membranes are ~ 3.453 and 2.137 mg/mL, respectively. This means the pure BC membranes and BC-CNT-PPy composite membranes have the same degradation efficiency at the fourth hour. Judging from the reducing sugar and total sugar content, their degradation degree of BC and BC-CNT-PPy is almost the same. However, as observed in Fig. 4c, the total sugar content for BC degradation is lower than that for BC-CNT-PPy, which may be attributed to that the initial total sugar content of BC is lower than that for BC-CNT-PPy. This is generally caused by the systematic errors during measurement, which is consistent with previous literatures [72]. Interestingly, from Fig. 4a and 4b, the BC-CNT-PPy composite membranes maintain more integrity structure compared with the pure BC membranes at the fourth hour of degradation. This is attributed to the formation of core-shell structure after coating PPy onto BC nanofiber, which can help to maintain the structure after the partial degradation of BC nanofibers. With further degradation process, the membrane tends to be fully cracked and left with only CNT and PPy particles in the end (Fig. 4b). Corresponding standard curves of total sugar and reducing sugar are shown in Fig. S7.

Based on the stability and high-output properties of the all-cellulose TENG, the TENG constructed from two different BC components can be used to drive low-power commercial electronics and work as a wearable cellulose interface. Fig. 5a and Movie S1 shows that the all-cellulose-TENG (based on BC-CNT-PPy with resistance of 0.3 k Ω) with a commercial bridge rectifier can easily light up seven light-emitting diodes in series (contact frequency at 3 Hz separation distance at 5 cm). External

mechanical energy can be readily converted into electrical energy by the all-cellulose TENG. To power various electronic devices, the harvested electrical energy needs to be stored for more efficient usage. Considering the pulse output characters of TENG, commercial capacitors with different capacitances are used for energy storage on demand in this work [7]. Fig. 5b depicts the charging process of the all-cellulose TENG to different capacitors through a bridge rectifier. It requires 4 , 10 , 52 , and 137 s to charge the capacitor of 2.2 , 10 , 47 , and 100 μF to 8 V, respectively. Smaller capacitor is easier and faster to be charged, while the larger capacitor can be used to drive high power electronics. For instance, the electronic watch (DFYJ.CO, NT-62, 3 μW) can be easily powered by the all-cellulose TENG charged 2.2 μF capacitor as shown in Fig. 5c and Movie S2. Capacitor (2.2 μF) charge and discharge curve when the all-cellulose TENG powers the electronic watch shown in Fig. S8. To drive a stopwatch with relatively higher power (M.Air, A-189, 10 μW), a paired capacitor of 47 μF charged by the all-cellulose TENG is needed (Fig. 5d). The stopwatch can be turned on at the 60th seconds (8 V) by the harvested mechanical energy through the BC TENG (Fig. S9 and Movie S3). The all-cellulose TENG is demonstrated to be fully capable of powering commercial electronic devices with different power consumptions.

Supplementary material related to this article can be found online at [doi:10.1016/j.nanoen.2021.106354](https://doi.org/10.1016/j.nanoen.2021.106354).

The harvested mechanical energy can also be used as a switch signal recognized by single-chip microcomputer to trigger a processing circuit and embedded software program. In this way, the all-cellulose TENG can be used as a eco-friendly wearable interface to control/trigger some

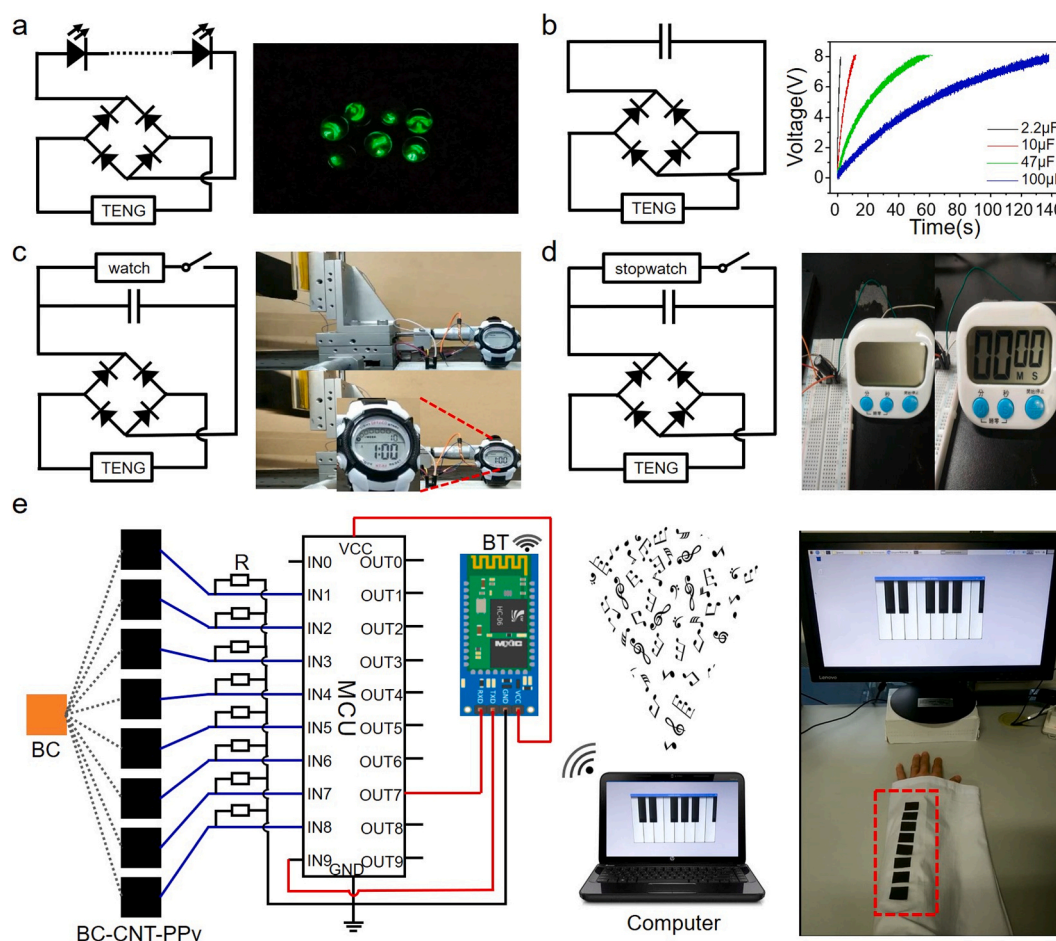


Fig. 5. The developed applications of the designed all cellulose TENG. (a) All cellulose TENG is successfully used as a direct current power source to light up 7 LEDs connected in series. All cellulose TENG powers the (b) capacitors, (c) watch, (d) stopwatch. (e) Schematic diagram of wearable electronic piano based on the all cellulose TENG.

software-level (or hardware-level) applications. As a proof of concept, we try to use eight BC-CNT-PPy TENGs in single electrode mode (Fig. S10) to functionalize as eight piano keys to play a simulated electronic piano and demonstrate the virtual keys in computer. As shown in Fig. 5e, eight BC-CNT-PPy TENGs are connected to the PIN 1 to PIN 8 through eight pull-down resistors, respectively. When the cellulose piano keys (i.e., BC-CNT-PPy TENGs) are touched by the fingers, electrons will flow from the ground to BC-CNT-PPy friction layer due to electrostatic induction to form a current flow, which will induce effective trigger signals to implement corresponding program to activate the music notes of Do, Re, Mi, Fa, Sol, La, Si and higher-tune Do, respectively. In details, the BC-CNT-PPy TENGs induce the analog triboelectric signals with an average voltage of ~ 0.5 V (Fig. S11), which can be recognized by the single-chip microcomputer (Arduino, available reading threshold voltage ranged from 0.005 to 5 V) and converted into digital signals. The digital signals are transmitted by the Bluetooth module (BT1) to another Bluetooth module (BT2) and received by the embedded program in computer to drive the corresponding music notes. The eight BC-CNT-PPy TENGs can also be readily sewed on the gusset and used as a wearable interface to play the music notes (Movie S4) and a melody of “Tinkerbell” (Movie S5). In addition, we have also tried to play a cyber game of “Greedy Snake” controlled by the all-cellulose TENG (Fig. 6a). We firstly mount pure BC membrane on thumb and BC-CNT-PPy membrane on index, middle, ring, and little fingers, respectively. The index, middle, ring, and little fingers control the “Greedy Snake” movement to the right, up, down and left, respectively.

The basic working process of TENG controlling “Greedy Snake” is shown in Fig. 6b. The TENG can generate an electrical signal by fingers touch, which can be received by Arduino and implement corresponding action order for the “Greedy Snake” to move toward target directions. Fig. 6c shows the detail of the movement process of the “Greedy Snake” triggered by finger touch via the all-cellulose TENG. Relevant experiment videos are shown in Movie S6. Furthermore, to satisfy more practical applications, we have also added the stability tests for the ordinary motions in the frequency of most cases in daily life, e.g., finger and all-cellulose TENG in touch frequency of once, twice, and three times within 1 s. The results are shown in Fig. S12, all the collected peak signals show a relatively stable situation and locate within the available reading threshold voltage range of Arduino (from 0.005 to 5 V). The demonstrated all-cellulose TENG is ready to drive commercial electronics and functionalize as wearable interfaces, which is also promising to be used for potential applications with biodegradable requirements.

Supplementary material related to this article can be found online at [doi:10.1016/j.nanoen.2021.106354](https://doi.org/10.1016/j.nanoen.2021.106354).

3. Conclusion

In summary, we have developed an eco-friendly energy-harvesting and interactive device based on all-cellulose composites. Energy-harvesting relies on the all-cellulose TENG, which exhibits the maximum open-circuit voltage of 29 V, short-circuit current of $0.6 \mu\text{A}$, and output power at $3 \mu\text{W}$. The demonstrated output power enables to

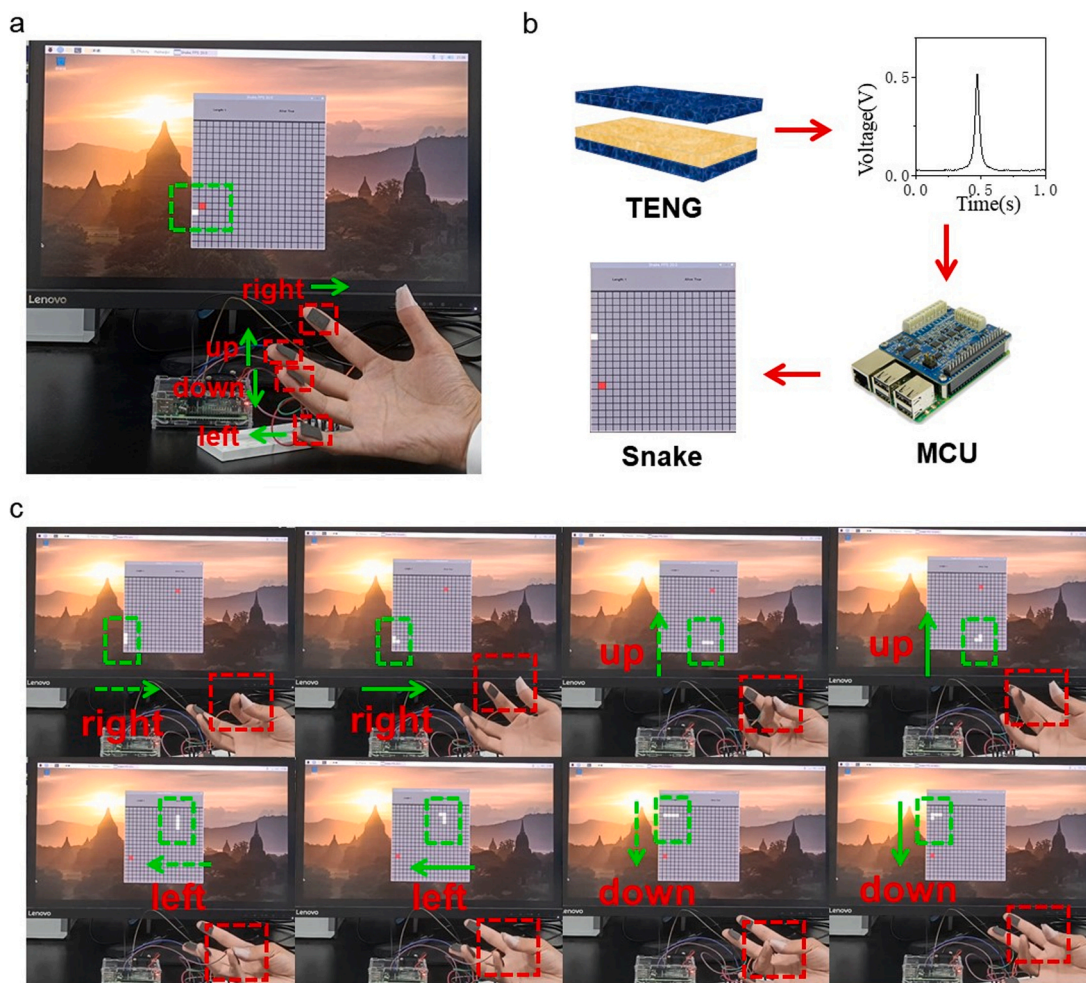


Fig. 6. Fingertip control “Greedy Snake” based on the all-cellulose TENG. (a) The index, middle, ring and little fingers control the “Greedy Snake” movement to right, up, down and left, respectively. (b) the basic working process of TENG controlling the “Greedy Snake”. (c) “Greedy Snake” cyber game triggered by the fingers via all-cellulose TENG.

drive commercial electronics, and the output signals can be directly used as the trigger signal for human-computer interaction to control a sewable electronic piano. The biodegradation experiments are also conducted to demonstrate that BC and BC-CNT-PPy membranes can be degraded within 8 h and the left CNTs can be cycled to use. As BC is a typical biopolymer produced by bacteria, it also shows advantage of high purity, high porosity, permeability to liquid/gas, good biocompatibility, mechanical robustness and facile to be doped with conductive materials. Combining BC with efficient energy-harvesting TENG shows huge potential in implanted electronics, transient energy devices, biological safety human-machine interface and bio-adaptable electronic devices for artificial tissues/organs.

4. Experiments

4.1. Materials

The bacterial cellulose (BC) pellicles purchased from Hainan Yide Foods Co. Ltd. (China). The short multi-walled carbon nanotubes (MWCNTs, purity ≥ 98 wt%, length = 0.5–2 μm) were purchased from Chengdu Organic Chemicals Co. Ltd. The rest of materials such as cetyl trimethyl-ammonium bromide (CTAB), $\text{FeCl}_3 \cdot 6\text{H}_2\text{O}$, Pyrrole with 98% of purity, P-toluenesulfonic acid (PTSA) were supplied by Aladdin and used without further purification.

4.2. Characterizations

The morphologies of membranes were observed using S-4800 field emission scanning electron microscope (FE-SEM). Thermal gravimetric analysis (TGA) was carried out under nitrogen atmosphere with by using the thermogravimetric analyzer (Pyris1, China) in the temperature range of 5–700 $^\circ\text{C}$ at a heating rate of 10 $^\circ\text{C}/\text{min}$. The Fourier transform-infrared (FT-IR) spectra were recorded on a FTIR spectrometer (VERTEX80v, Bruker) using the pressing potassium bromide troche method [73]. The V_{OC} , I_{SC} , and Q_{SC} were measured by an electrometer (Keithley 6514 system). A custom LabVIEW program was used to record the electrical output.

4.3. Preparation of BC-CNT-PPy composite membranes

The BC-CNT-PPy composite membranes were prepared in a two-step reaction, first grafting reinforcement with CNT with a doping process (BC-CNT), followed by in-situ oxidative polymerization of pyrrole (BC-CNT-PPy). The BC pellicles were cut into a size of 6 cm \times 6 cm, then washed thoroughly with distilled water until PH = 7 and changed into a swollen state. The CNT were dispersed in pure water (0.2 wt%) with a cationic CTAB (0.4 wt% in water) to obtain the MWCNT dispersion. Ultrasonication was then applied to the MWCNT dispersion with a nominal frequency of 28 kHz and a power of 600 W for 1 h at 25 $^\circ\text{C}$ to stabilize them against van der Waals attraction. The highly swollen BC was immersed in the MWCNTs dispersion, ultrasonication for 1 h at room temperature, then oscillation at 150 rpm/sec for 23 h, and this procedure is repeated for three times. In this way, the MWCNTs could be well-dispersed in the bacterial cellulose to obtain the BC-CNT composite pellicles. The BC-CNT composite pellicles were rinsed several times in distilled water to remove surfactants. After mechanical pressing to remove the physically adsorbed water, the MWCNT-doped BC pellicles were immersed in the aqueous solution of iron (III) chloride hexahydrate ($\text{FeCl}_3 \cdot 6\text{H}_2\text{O}$) with concentration 0.1 mol/L under magnetic stirring for 2 h, then withdrew and immersed in the pyrrole solution with PTSA, the molar ratio of $\text{FeCl}_3 \cdot 6\text{H}_2\text{O}:\text{PPy}:\text{PTSA}$ was 2.6:1:1. Here, iron (III) chloride hexahydrate is an oxidant for the in-situ oxidative polymerization of pyrrole to PPy. The mixture was placed inside the refrigerator at 4 ± 1 $^\circ\text{C}$ for 60 min to initiate the polymerization of polypyrrole and obtain BC-CNT-PPy composite pellicles. After the reaction completed, the obtained composite pellicles were washed with distilled water to

remove excess agents. Finally, the BC-CNT-PPy composite membranes were prepared by hot-pressing the composite pellicles under 120 $^\circ\text{C}$ for 6 h. The pure BC membranes were also prepared with the hot-pressing method.

Declaration of Competing Interest

The authors declare that they have no known competing financial interests or personal relationships that could have appeared to influence the work reported in this paper.

Acknowledgements

This work is financially supported by the National Key Research and Development Program of China (2016YFA0202703), the National Natural Science Foundation of China (52073031, 51973076, 21774039), the Fundamental Research Funds for the Central Universities (E0EG6801X2), Beijing Nova Program (Z191100001119047), the ‘‘Hundred Talents Program’’ of the Chinese Academy of Sciences.

Appendix A. Supporting information

Supplementary data associated with this article can be found in the online version at [doi:10.1016/j.nanoen.2021.106354](https://doi.org/10.1016/j.nanoen.2021.106354).

References

- [1] F.-R. Fan, Z.-Q. Tian, Z. Lin Wang, Flexible triboelectric generator, *Nano Energy* 1 (2012) 328–334.
- [2] Y. Zi, H. Guo, Z. Wen, M.H. Yeh, C. Hu, Z.L. Wang, Harvesting low-frequency (<5 Hz) irregular mechanical energy: a possible killer application of triboelectric nanogenerator, *ACS Nano* 10 (2016) 4797–4805.
- [3] Z.L. Wang, On Maxwell's displacement current for energy and sensors: the origin of nanogenerators, *Mater. Today* 20 (2017) 74–82.
- [4] Y. Tang, H. Zhou, X. Sun, N. Diao, J. Wang, B. Zhang, C. Qin, E. Liang, Y. Mao, Triboelectric touch-free screen sensor for noncontact gesture recognizing, *Adv. Funct. Mater.* 30 (2020), 1907893.
- [5] H. Guo, X. Pu, J. Chen, Y. Meng, M.-H. Yeh, G. Liu, Q. Tang, B. Chen, D. Liu, S. Qi, C. Wu, C. Hu, J. Wang, Z.L. Wang, A highly sensitive, self-powered triboelectric auditory sensor for social robotics and hearing aids, *Sci. Robot.* 3 (2018) eaat2516.
- [6] X. Pu, H. Guo, J. Chen, X. Wang, Y. Xi, C. Hu, Z.L. Wang, Eye motion triggered self-powered mechnosensational communication system using triboelectric nanogenerator, *Sci. Adv.* 3 (2017), e1700694.
- [7] C. Zhao, Q. Zhang, W. Zhang, X. Du, Y. Zhang, S. Gong, K. Ren, Q. Sun, Z.L. Wang, Hybrid piezo/triboelectric nanogenerator for highly efficient and stable rotation energy harvesting, *Nano Energy* 57 (2019) 440–449.
- [8] S. Xiang, D. Liu, C. Jiang, W. Zhou, D. Ling, W. Zheng, X. Sun, X. Li, Y. Mao, C. Shan, Liquid-metal-based dynamic thermoregulating and self-powered electronic skin, *Adv. Funct. Mater.* 31 (2021), 2100940.
- [9] J. Huang, X. Yang, J. Yu, J. Han, C. Jia, M. Ding, J. Sun, X. Cao, Q. Sun, Z.L. Wang, A universal and arbitrary tactile interactive system based on self-powered optical communication, *Nano Energy* 69 (2020), 104419.
- [10] J. Han, C. Xu, J. Zhang, N. Xu, Y. Xiong, X. Cao, Y. Liang, L. Zheng, J. Sun, J. Zhai, Q. Sun, Z.L. Wang, Multifunctional coaxial energy fiber toward energy harvesting, storage, and utilization, *ACS Nano* 15 (2021) 1597–1607.
- [11] Y. Yang, J. Han, J. Huang, J. Sun, Z.L. Wang, S. Seo, Q. Sun, Stretchable energy-harvesting tactile interactive interface with liquid-metal-nanoparticle-based electrodes, *Adv. Funct. Mater.* 30 (2020), 1909652.
- [12] D.H. Ho, J. Han, J. Huang, Y.Y. Choi, S. Cheon, J. Sun, Y. Lei, G.S. Park, Z.L. Wang, Q. Sun, J.H. Cho, β -phase-preferential blow-spun fabrics for wearable triboelectric nanogenerators and textile interactive interface, *Nano Energy* 77 (2020), 105262.
- [13] H. Kang, C. Zhao, J. Huang, D.H. Ho, Y.T. Megra, J.W. Suk, J. Sun, Z.L. Wang, Q. Sun, J.H. Cho, Fingerprint-inspired conducting hierarchical wrinkles for energy-harvesting E-skin, *Adv. Funct. Mater.* 29 (2019), 1903580.
- [14] G. Gao, B. Wan, X. Liu, Q. Sun, X. Yang, L. Wang, C. Pan, Z.L. Wang, Tunable tribotronic dual-gate logic devices based on 2D MoS_2 and black phosphorus, *Adv. Mater.* 30 (2018), 1705088.
- [15] Y. Meng, J. Zhao, X. Yang, C. Zhao, S. Qin, J.H. Cho, C. Zhang, Q. Sun, Z.L. Wang, Mechanosensation-active matrix based on direct-contact tribotronic planar graphene transistor array, *ACS Nano* 12 (2018) 9381–9389.
- [16] J. Yu, X. Yang, Q. Sun, Piezo/tribotronics toward smart flexible sensors, *Adv. Intell. Syst.* 2 (2020), 1900175.
- [17] M. Jia, J. Yu, Y. Liu, P. Guo, Y. Lei, W. Wang, A. Yu, Y. Zhu, Q. Sun, J. Zhai, Z. L. Wang, Multibit tribotronic nonvolatile memory based on van der Waals heterostructures, *Nano Energy* 83 (2021), 105785.
- [18] G. Gao, J. Yu, X. Yang, Y. Pang, J. Zhao, C. Pan, Q. Sun, Z.L. Wang, Tribotronic transistor of MoS_2 , *Adv. Mater.* 31 (2019), e1806905.

- [19] X. Yang, J. Han, J. Yu, Y. Chen, H. Zhang, M. Ding, C. Jia, J. Sun, Q. Sun, Z. L. Wang, Versatile triboiontronic transistor via proton conductor, *ACS Nano* 14 (2020) 8668–8677.
- [20] H. Zhang, J. Yu, X. Yang, G. Gao, S. Qin, J. Sun, M. Ding, C. Jia, Q. Sun, Z.L. Wang, Ion gel capacitively coupled tribotronic gating for multiparameter distance sensing, *ACS Nano* 14 (2020) 3461–3468.
- [21] X. Yang, J. Yu, J. Zhao, Y. Chen, G. Gao, Y. Wang, Q. Sun, Z.L. Wang, Mechanoplastic tribotronic floating-gate neuromorphic transistor, *Adv. Funct. Mater.* 30 (2020), 2002506.
- [22] Y. Chen, G. Gao, J. Zhao, H. Zhang, J. Yu, X. Yang, Q. Zhang, W. Zhang, S. Xu, J. Sun, Y. Meng, Q. Sun, Piezotronic graphene artificial sensory synapse, *Adv. Funct. Mater.* 29 (2019), 1900959.
- [23] J. Wang, Y. Chen, L.-A. Kong, Y. Fu, Y. Gao, J. Sun, Deep-ultraviolet-triggered neuromorphic functions in In-Zn-O phototransistors, *Appl. Phys. Lett.* 113 (2018), 151101.
- [24] J. Sun, Y. Fu, Q. Wan, Organic synaptic devices for neuromorphic systems, *J. Phys. D Appl. Phys.* 51 (2018), 314004.
- [25] C. Qian, J. Sun, L.-a Kong, Y. Fu, Y. Chen, J. Wang, S. Wang, H. Xie, H. Huang, J. Yang, Y. Gao, Multilevel nonvolatile organic photomemory based on vanadyl-phthalocyanine/para-sexiphenyl heterojunctions, *ACS Photon.* 4 (2017) 2573–2579.
- [26] C. Qian, L.-a Kong, J. Yang, Y. Gao, J. Sun, Multi-gate organic neuron transistors for spatiotemporal information processing, *Appl. Phys. Lett.* 110 (2017), 083302.
- [27] L.-a Kong, J. Sun, C. Qian, Y. Fu, J. Wang, J. Yang, Y. Gao, Long-term synaptic plasticity simulated in ionic liquid/polymer hybrid electrolyte gated organic transistors, *Org. Electron.* 47 (2017) 126–132.
- [28] L.-a Kong, J. Sun, C. Qian, C. Wang, J. Yang, Y. Gao, Spatially-correlated neuron transistors with ion-gel gating for brain-inspired applications, *Org. Electron.* 44 (2017) 25–31.
- [29] B. Zhang, Y. Tang, R. Dai, H. Wang, X. Sun, C. Qin, Z. Pan, E. Liang, Y. Mao, Breath-based human-machine interaction system using triboelectric nanogenerator, *Nano Energy* 64 (2019), 103953.
- [30] N. Zhang, C. Qin, T. Feng, J. Li, Z. ang, X.; E. Sun, Y. Mao, X. Wang, Non-contact cylindrical rotating triboelectric nanogenerator for harvesting kinetic energy from hydraulics, *Nano Res* 13 (2020) 1903–1907.
- [31] H. Guo, X. Pu, C. Jie, M. Yan, Y. Min-Hsin, G. Liu, A highly sensitive, self-powered triboelectric auditory sensor for social robotics and hearing aids, *Sci. Robot.* 3 (2018), eaat2516.
- [32] Z. Lin, B. Zhang, H. Guo, Z. Wu, Z.L. Wang, Super-robust and frequency-multiplied triboelectric nanogenerator for efficient harvesting water and wind energy, *Nano Energy* 64 (2019), 103908.
- [33] G. Liu, L. Xiao, C. Chen, W. Liu, Z.L. Wang, Power cables for triboelectric nanogenerator networks for large-scale blue energy harvesting, *Nano Energy* 75 (2020), 104975.
- [34] H. Zou, Y. Zhang, L. Guo, P. Wang, X. He, G. Dai, H. Zheng, C. Chen, A.C. Wang, C. Xu, Z.L. Wang, Quantifying the triboelectric series, *Nat. Commun.* 10 (2019) 1427.
- [35] L. Zhang, Y. Liao, Y.C. Wang, S. Zhang, W. Yang, X. Pan, Z.L. Wang, Cellulose II aerogel-based triboelectric nanogenerator, *Adv. Funct. Mater.* 30 (2020), 2001763.
- [36] M. Wang, J. Zhang, Y. Tang, J. Li, B. Zhang, E. Liang, Y. Mao, X. Wang, Air flow-driven triboelectric nanogenerators for self-powered real-time respiratory monitoring, *ACS Nano* 12 (2018) 6156–6162.
- [37] X. Peng, K. Dong, C. Ye, Y. Jiang, S. Zhai, R. Cheng, D. Liu, X. Gao, J. Wang, Z. L. Wang, A breathable, biodegradable, antibacterial, and self-powered electronic skin based on all-nanofiber triboelectric nanogenerators, *Sci. Adv.* 6 (2020), eaab9624.
- [38] Y. Lu, X. Li, J. Ping, J. s He, J. Wu, A flexible, recyclable, and high-performance pullulan-based triboelectric nanogenerator (TENG), *Adv. Mater. Technol.* 5 (2019), 1900905.
- [39] Z. Bai, Y. Xu, J. Li, J. Zhu, C. Gao, Y. Zhang, J. Wang, J. Guo, An eco-friendly porous nanocomposite fabric-based triboelectric nanogenerator for efficient energy harvesting and motion sensing, *ACS Appl. Mater. Interfaces* 12 (2020) 42880–42890.
- [40] Y. Mao, N. Zhang, Y. Tang, M. Wang, M. Chao, E. Liang, A paper triboelectric nanogenerator for self-powered electronic systems, *Nanoscale* 9 (2017) 14499–14505.
- [41] K. Xia, J. Fu, Z. Xu, Multiple-Frequency high-output triboelectric nanogenerator based on a water balloon for all-weather water wave energy harvesting, *Adv. Energy Mater.* 10 (2020), 2000426.
- [42] K. Xia, Z. Zhu, H. Zhang, C. Du, Z. Xu, R. Wang, Painting a high-output triboelectric nanogenerator on paper for harvesting energy from human body motion, *Nano Energy* 50 (2018) 571–580.
- [43] R. Zhang, C. Dahlström, H. Zou, J. Jonzon, M. Hummelgård, J. Örtengren, N. Blomquist, Y. Yang, H. Andersson, M. Olsen, M. Norgren, H. Olin, Z.L. Wang, Cellulose-Based fully green triboelectric nanogenerators with output power density of 300 W m⁻², *Adv. Mater.* 32 (2020), 2002824.
- [44] Q. Zheng, Y. Zou, Y. Zhang, Z. Liu, B. Shi, X. Wang, Y. Jin, H. Ouyang, Z. Li, Z. L. Wang, Biodegradable triboelectric nanogenerator as a life-time designed implantable power source, *Sci. Adv.* 2 (2016), e1501478.
- [45] Z. Liu, H. Li, B. Shi, Y. Fan, Z.L. Wang, Z. Li, Wearable and implantable triboelectric nanogenerators, *Adv. Funct. Mater.* 29 (2019), 1808820.
- [46] Q. Zheng, Q. Tang, Z.L. Zhong Lin Wang, Z. Li, Self-powered cardiovascular electronic devices and systems, *Nat. Rev. Cardiol.* 18 (2021) 7–21.
- [47] P. Maharjan, R.M. Toyabur, J.Y. Park, A human locomotion inspired hybrid nanogenerator for wrist-wearable electronic device and sensor applications, *Nano Energy* 46 (2018) 383–395.
- [48] H. Ouyang, Z. Liu, N. Li, B. Shi, Y. Zou, F. Xie, Y. Ma, Z. Li, H. Li, Q. Zheng, X. Qu, Y. Fan, Z.L. Wang, H. Zhang, Z. Li, Symbiotic cardiac pacemaker, *Nat. Commun.* 10 (2019) 1821.
- [49] Y. Chi, K. Xia, Z. Zhu, J. Fu, H. Zhang, C. Du, Z. Xu, Rice paper-based biodegradable triboelectric nanogenerator, *Microelectron. Eng.* 216 (2019), 111059.
- [50] W. Jiang, H. Li, Z. Liu, Z. Li, J. Tian, B. Shi, Y. Zou, H. Ouyang, C. Zhao, L. Zhao, R. Sun, H. Zheng, Y. Fan, Z.L. Wang, Z. Li, Fully bioabsorbable natural-materials-based triboelectric nanogenerators, *Adv. Mater.* 30 (2018), 1801895.
- [51] K. Xia, D. Wu, J. Fu, N.A. Hoque, Y. Ye, Z. Xu, Tunable output performance of triboelectric nanogenerator based on alginate metal complex for sustainable operation of intelligent keyboard sensing system, *Nano Energy* 78 (2020), 105263.
- [52] K. Shi, X. Huang, B. Sun, Z. Wu, J. He, P. Jiang, Cellulose/BaTiO₃ aerogel paper based flexible piezoelectric nanogenerators and the electric coupling with triboelectricity, *Nano Energy* 57 (2019) 450–458.
- [53] I. Kim, H. Jeon, D. Kim, J. You, D. Kim, All-in-one cellulose based triboelectric nanogenerator for electronic paper using simple filtration process, *Nano Energy* 53 (2018) 975–981.
- [54] C. Qian, L. Li, M. Gao, H. Yang, Z. Cai, B. Chen, Z. Xiang, Z. Zhang, Y. Song, All-printed 3D hierarchically structured cellulose aerogel based triboelectric nanogenerator for multi-functional sensors, *Nano Energy* 63 (2019), 103885.
- [55] R.R. AM, Y. Liu, C. Liu, K.H. Schafer, M. Saumer, G. Yang, Carbon nanotube-reinforced poly(4-vinylaniline)/polyaniline bilayer-grafted bacterial cellulose for bioelectronic applications, *ACS Biomater. Sci. Eng.* 5 (2019) 2160–2172.
- [56] Z. Shi, Y. Li, X. Chen, H. Han, G. Yang, Double network bacterial cellulose hydrogel to build a biology-device interface, *Nanoscale* 6 (2014) 970–977.
- [57] A. Jasim, M.W. Ullah, Z. Shi, X. Lin, G. Yang, Fabrication of bacterial cellulose/polyaniline/single-walled carbon nanotubes membrane for potential application as biosensor, *Carbohydr. Polym.* 163 (2017) 62–69.
- [58] L. Wang, S. Hu, M.W. Ullah, X. Li, Z. Shi, G. Yang, Enhanced cell proliferation by electrical stimulation based on electroactive regenerated bacterial cellulose hydrogels, *Carbohydr. Polym.* 249 (2020), 116829.
- [59] S. Wang, T. Li, C. Chen, W. Kong, S. Zhu, J. Dai, A.J. Diaz, E. Hitz, S.D. Solares, T. Li, L. Hu, Transparent, anisotropic biofilm with aligned bacterial cellulose nanofibers, *Adv. Funct. Mater.* 28 (2018), 1707491.
- [60] A. Nakayama, A. Kakugo, J.P. Gong, Y. Osada, M. Takai, T. Erata, S. Kawano, High mechanical strength double-network hydrogel with bacterial cellulose, *Adv. Funct. Mater.* 14 (2004) 1124–1128.
- [61] S.-S. Kim, J.-H. Jeon, H.-I. Kim, C.D. Kee, I.-K. Oh, High-fidelity bioelectronic muscular actuator based on graphene-mediated and TEMPO-oxidized bacterial cellulose, *Adv. Funct. Mater.* 25 (2015) 3560–3570.
- [62] O. Eskilson, S.B. Lindström, B. Sepulveda, M.M. Shahjamali, P. Güell-Grau, P. Sivlér, M. Skog, C. Aronsson, E.M. Björk, N. Nyberg, H. Khalaf, T. Bengtsson, J. James, M.B. Ericson, E. Martinsson, R. Selegård, D. Aili, Self-assembly of mechanoplasmonic bacterial cellulose-metal nanoparticle composites, *Adv. Funct. Mater.* 30 (2020), 2004766.
- [63] C. Long, D. Qi, T. Wei, J. Yan, L. Jiang, Z. Fan, Nitrogen-doped carbon networks for high energy density supercapacitors derived from polyaniline coated bacterial cellulose, *Adv. Funct. Mater.* 24 (2014) 3953–3961.
- [64] F. Wang, Q. Li, J.O. Park, S. Zheng, E. Choi, Ultralow voltage high-performance bioartificial muscles based on ionically crosslinked polypyrrole-coated functional carboxylated bacterial cellulose for soft robots, *Adv. Funct. Mater.* (2020), 2007749.
- [65] M. Florea, B. Reeve, J. Abbott, P.S. Freemont, T. Ellis, Genome sequence and plasmid transformation of the model high-yield bacterial cellulose producer *Gluconacetobacter hansenii* ATCC 53582, *Sci. Rep.* 6 (2016) 23635.
- [66] L. Ma, R. Liu, H. Niu, F. Wang, L. Liu, Y. Huang, Freestanding conductive film based on polypyrrole/bacterial cellulose/graphene paper for flexible supercapacitor: large areal mass exhibits excellent areal capacitance, *Electrochim. Acta* 222 (2016) 429–437.
- [67] C. Xu, B. Zhang, A.C. Wang, W. Cai, Y. Zi, P. Feng, Z.L. Wang, Effects of metal work function and contact potential difference on electron thermionic emission in contact electrification, *Adv. Funct. Mater.* 29 (2019), 1903142.
- [68] C. Xu, Y. Zi, A.C. Wang, H. Zou, Y. Dai, X. He, P. Wang, Y.C. Wang, P. Feng, D. Li, Z. L. Wang, On the electron-transfer mechanism in the contact-electrification effect, *Adv. Mater.* 30 (2018), 1706790.
- [69] S. Niu, S. Wang, L. Lin, Y. Liu, Y.S. Zhou, Y. Hu, Theoretical study of contact-mode triboelectric nanogenerators as an effective power source, *Energy Environ. Sci.* 6 (2018) 3576–3583.
- [70] M. Samegima, J. Sugiyama, K. Igarashi, k Eriksson, Enzymatic hydrolysis of bacterial cellulose, *Carbohydr. Res.* 305 (1998) 281–288.
- [71] T.M. Woods, S.I. McCrae, Synergism between enzymes involved in solubilization of native cellulose, *Adv. Chem. Ser.* 181 (1979) 181–209.
- [72] L. Mao, S. Hu, Y. Cao, L. Wang, W. Zhao, L. Fu, H. Chen, L. Xia, S. Xie, W. Ye, Z. Shi, G. Yang, Biodegradable and electroactive regenerated bacterial cellulose/MXene (Ti₃C₂T_x) composite hydrogel as wound dressing for accelerating skin wound healing under electrical stimulation, *Adv. Healthc. Mater.* 9 (2020), 2000872.
- [73] L. Tang, J. Han, Z. Jiang, S. Chen, H. Wang, Flexible conductive polypyrrole nanocomposite membranes based on bacterial cellulose with amphiphobicity, *Carbohydr. Polym.* 117 (2015) 230–235.